JGR Oceans

RESEARCH ARTICLE
10.1029/2019JC015342

Key Points:
- Equatorial Indian Ocean semiannual velocity and isotherm displacement variability are analyzed using Argo data
- Zonal and meridional velocity at 1,000 dbar as well as isotherm displacements are consistent with Rossby wave physics
- The 3-D isotherm displacement structure suggests a vertically propagating Rossby wave

Correspondence to:
H. Zanowski,
hannah.zanowski@colorado.edu

Citation:
Zanowski, H., & Johnson, G. C. (2019). Semiannual variations in 1,000-dbar equatorial Indian Ocean velocity and isotherm displacements from Argo data. *Journal of Geophysical Research: Oceans*, *124*, 9507–9516. https://doi.org/10.1029/2019JC015342

Received 31 MAY 2019
Accepted 8 DEC 2019
Accepted article online 19 DEC 2019
Published online 24 DEC 2019

Semiannual Variations in 1,000-dbar Equatorial Indian Ocean Velocity and Isotherm Displacements from Argo Data

Hannah Zanowski[1] and Gregory C. Johnson[2]

[1]Joint Institute for the Study of the Atmosphere and Ocean, University of Washington, Seattle, WA, USA, [2]NOAA/Pacific Marine Environmental Laboratory, Seattle, WA, USA

Abstract The semiannual Rossby wave in the equatorial Indian Ocean is analyzed using 1,000-dbar horizontal drift and 3-D isotherm displacement data from Argo floats. The strong semiannual variations in zonal velocity associated with this wave that have been previously studied are confirmed here, and a more complete picture of the wave is provided with the addition of the 1,000-dbar meridional velocities and 0- to 2,000-dbar isotherm displacements. At 1,000 dbar, semiannual variations in each field are consistent with Rossby wave physics: Zonal velocity is maximal on the equator, isotherm displacement and meridional velocity extrema are colocated with equatorially symmetric zonal velocity phase reversals near ±2.5° in latitude, and all three fields propagate westward over the year. The latitudinal structure of the meridional velocities in the central and eastern Indian Ocean hints at Rossby wave energy in higher meridional modes than the first, but that signature is not apparent in the isotherm displacements or the zonal velocities. With upward and westward phase propagation and downward and westward energy propagation, isotherm displacement vertical sections confirm the presence of a vertically propagating wave that reaches to at least 2,000 dbar, the deepest extent of the Argo floats.

Plain Language Summary The currents in the equatorial Indian Ocean vary on many different timescales, from months to decades. Changes that occur semiannually, or twice a year, are particularly strong in this region. At the surface, the currents vary in this way because the Asian monsoon causes the winds to reverse direction semiannually. Below the surface, changes in the currents are due in part to long, planetary-scale waves, known as Rossby and Kelvin waves, that travel both horizontally and vertically in the ocean, in this case trapped along the equator. Here semiannual changes in tropical Indian Ocean currents at 1,000 m are examined using velocity and isotherm displacement (changes in the depth of constant temperature surfaces) data from Argo floats. In agreement with earlier studies, these data show that Rossby waves are responsible for much of the prominent semiannual variation in the deep east-west velocities and isotherm displacements. The floats also allow detection of the much subtler semiannual reversals in north-south velocities on either side of the equator associated with these Rossby waves. By exploring isotherm displacement changes in depth versus both longitude and latitude, it is also shown that the Rossby wave travels vertically, as expected.

1. Introduction

The equatorial Indian Ocean hosts a complex, spatially and temporally varying circulation. While it is composed of some features typical of the equatorial oceans—for example, an eastward flowing equatorial countercurrent (here the South Equatorial Counter Current) near the surface (e.g., Schott & McCreary, 2001), an Equatorial Undercurrent (e.g., Knox, 1974) below, and extending deeper still, equatorial deep jets (e.g., Dengler & Quadfasel, 2002; Luyten & Swallow, 1976; Ponte & Luyten, 1990; Youngs & Johnson, 2015)—there are several aspects of the circulation and its forcing that are unique to the Indian Ocean. Unlike in the equatorial Atlantic and Pacific oceans, the equatorial Indian Ocean circulation is strongly influenced by the Asian monsoon (e.g., Schott et al., 2009; Schott & McCreary, 2001). As such, many of the currents, including the Equatorial Undercurrent, are not permanent features of the circulation and have been observed to reverse and/or disappear due to seasonal wind variations (Iskandar et al., 2009; Knox, 1976; Knox & Anderson, 1985; Reppin et al., 1999; Wyrtki, 1973). Some currents, such as the seasonally reversing Wyrtki Jets (Wyrtki, 1973), are found nowhere else. Although observations and models indicate that equatorial Indian Ocean currents vary across a broad range of timescales (Chen et al., 2015; Chen et al., 2019;

McPhaden et al., 2015; Nagura & McPhaden, 2008, 2010a, 2010b, 2016; Nyadjro & McPhaden, 2014; Sengupta et al., 2007; Visbeck & Schott, 1992; Zhang et al., 2014), it is the monsoonally driven, semiannual variations that are particularly robust in this region, including the strong eastward flowing Wyrtki jets during the spring and autumn monsoon transitions and the seasonally reversing western boundary current off Somalia (e.g., Davis, 2005; Han et al., 1999; Huang, McPhaden, et al., 2018; Luyten & Roemmich, 1982; Reverdin, 1987; Schott et al., 2009; Schott & McCreary, 2001; Visbeck & Schott, 1992; Wyrtki, 1973).

Directly forced and boundary-reflected Kelvin and Rossby waves play an important role in equatorial Indian Ocean current variability. While many studies have examined the impact of these waves on currents in the near-surface Indian Ocean (e.g., Han et al., 1999; Moore & McCreary, 1990; Nagura & McPhaden, 2016; Nyadjro & McPhaden, 2014; Yuan & Han, 2006), less is known about their impact below the thermocline. In their observational studies, both Luyten and Roemmich (1982) and Mcphaden (1982) found that semiannual variations in zonal velocity below the thermocline exhibited upward and westward phase propagation—an indication of the presence of vertically propagating Rossby waves. Modeling studies confirmed these observations (Gent et al., 1983; Jensen, 1993; Visbeck & Schott, 1992), although Gent et al. (1983) argued that the sub-thermocline semiannual zonal velocity phase propagation resulted from the sum of many standing vertical modes rather than vertically propagating waves. Building on the theoretical work of Cane and Moore (1981), Jensen's (1993) study also indicated the importance of basin resonance at the semiannual timescale in modulating equatorial Indian Ocean currents. Using a 3.5-layer model, Jensen (1993) showed that boundary-reflected, second baroclinic mode Kelvin and Rossby waves can constructively interfere with the semiannual wind-forced current response to create a semiannual basin resonance. Subsequent observational and modeling studies (e.g., Han et al., 1999; Han et al., 2011; Huang, Han, et al., 2018) have corroborated this.

Recently, Huang, McPhaden, et al. (2018) presented evidence from a combination of moorings and ocean reanalysis data from ORAS4 in support of the Luyten and Roemmich (1982) and McPhaden (1982) observations. They showed that semiannual variations in equatorial Indian Ocean middepth (500–1,500 m) zonal currents are due in part to vertically propagating Rossby waves that develop as a result of surface-wind forced Kelvin waves reflecting off the Indian Ocean's eastern boundary. In a separate study using a linear ocean model and ORAS4 reanalysis output, Huang, Han, et al. (2018) also indicated that basin resonance modulates equatorial Indian Ocean middepth currents, particularly the Equatorial Intermediate Current.

Using Argo data, here we provide independent confirmation of these results and, in addition to the zonal velocities, expand upon the work of Huang, McPhaden, et al. (2018) by examining 1,000-dbar meridional velocity and 0- to 2,000-dbar isotherm displacements as well. We find that there are also clear variations in the meridional velocity and isotherm displacements, especially in the eastern Indian Ocean, consistent with the presence of a vertically propagating semiannual Rossby wave there.

2. Data and Methods

The velocity and isotherm displacement fields used in this study are derived from Argo data updated through October 2018. Zonal and meridional velocities at 1,000 dbar are from YoMaHa'07 (Lebedev et al., 2007) and isotherm displacements from the monthly, 1° × 1°-gridded Argo Climatology (Roemmich & Gilson, 2009). The YoMaHa'07 velocities extend back to 1997, while the Argo Climatology begins in 2004. Velocities are mapped on a 0.25°lat. × 1.0°long. grid using a quadratic Loess filter with 2° meridional and 10° zonal scales. Both annual and semiannual harmonics are included in the fit, following Ridgway et al. (2002). For further quality control, data falling outside 3 times the interquartile range at each point are discarded prior to mapping. The effective number (N_{eff}) of data points (given by the sum of the loess weights) for the velocity mapping at each grid point ranges from ~80–1860, with $N_{\mathrm{eff}} > 100$ for 96% of grid points and $N_{\mathrm{eff}} > 1{,}000$ for 65% of grid points. The isotherm displacements, denoted as p′, are computed from the Roemmich and Gilson (2009) in situ temperature fields, as temperature variations below the thermocline are largely due to the vertical motion of water parcels (e.g., Kessler & McCreary, 1993). These data are first converted to potential temperature and then scaled by the local vertical temperature gradient, resulting in an isotherm displacement field in pressure units (dbar). The isotherm displacements are then fit with a mean and annual and semiannual harmonics at each grid point. For the semiannual harmonics, regions with fit amplitudes less than 1 cm·s^{-1} for zonal velocity, 0.2 cm·s^{-1} for meridional velocity, and 5 dbar for isotherm displacements are not shown. The

choice of these thresholds is empirical, guided both by the fact that they are 10–15% of the maximum amplitudes mapped and by visual assessment of noise in phase contours.

Theoretical Wentzel–Kramers–Brillouin (WKB) raypaths for nth meridional mode Rossby waves are also computed. From Appendix A of Kessler and McCreary (1993), the slopes of the rays are

$$\frac{dz}{dx} = \frac{(2n+1)\omega}{N(z)},$$

where ω is the frequency (semiannual in this case) and $N(z)$ the mean Brünt-Väisälä (buoyancy) frequency profile. The mean $N(z)$ profile is a zonal and latitudinal (3.5°S to 3.5°N) average of $N(z)$ computed from the Roemmich and Gilson (2009) mean temperature and salinity fields in the Indian Ocean. Zonal (k) and vertical (m) wavenumbers of the semiannual signals are estimated using $k = \omega/c_{px}$, where c_{px} is the zonal phase speed of the anomalies, and $m = kN/\omega(2n+1)$, where N is the depth-averaged Brünt-Väisälä frequency.

3. Results

3.1. The Mean

The mean 1,000-dbar zonal (u) and meridional (v) velocity fields show some coherent structures (Figure 1), but they are of fairly small amplitude and not basin length in scale. The mean zonal velocities (Figure 1a) typically range from 1–5 cm·s^{-1}. Between 7°S and 5°N, there are zonal jet-like structures of ~15°–30° in longitudinal extent, but they are much less coherent and weaker than similar features found in the Pacific (e.g., Cravatte et al., 2012). The mean meridional velocities are much weaker than the zonal, with magnitudes of 0.5–2 cm·s^{-1}, and they do not exhibit any coherent large-scale structure. The strongest zonal jet, flowing eastward from the African coast to about 60°E at 3°–4°S, is fed by meridional convergent flow along that coast. Additionally, where it shifts from 4°S to 3°S, there is northward flow, and where it fades from 55°–60°E there is a divergent meridional flow. Hence, the two fields, mapped independently, do indicate some continuity.

3.2. The Semiannual Harmonic

Semiannual variations in the equatorial 1,000-dbar horizontal velocity and isotherm displacement fields (Figure 2) are indicative of a Rossby wave. All three fields tend to show Rossby wave signals most clearly in the central and eastern Indian Ocean, east of 60°–65°E. The zonal velocity semiannual harmonic amplitude (Figure 2a) is maximal on the equator between 70°E and 85°E, with equatorially symmetric phase reversals (sharp meridional gradients in phase) at 2.5°N and 2.5°S. Along the equator, phase lines span ~150°. This result suggests that if a single wave was present, it would be larger than basin scale, although the presence of multiple waves, including reflected waves, could certainly modify the observed phase pattern. There is also some indication of another phase reversal at ~5°S between 75°E and 90°E, perhaps suggesting the presence of a higher meridional mode than the first. The meridional velocities (Figure 2b) exhibit their largest amplitudes (~1.5–2 cm·s^{-1}) in three regions: in the Northern Hemisphere along Somalia, in the southwestern Indian Ocean south of 7°S and west of 65°E, and off-equator between 80°E and 85°E. The off-equatorial anomalies in the eastern Indian Ocean are maximal at ±2°–±2.5° latitude, where the zonal velocities are small, and their phasing is asymmetric about the equator, again consistent with Rossby wave physics. The meridional velocities are also much smaller than the zonal velocities, as expected for long Rossby waves. In addition to the phase reversal on the equator, phase reversals near ±3.5°–±4° latitude occur in the meridional velocity field, also suggesting the presence of some energy at higher meridional modes than the first. Isotherm displacements (Figure 2c) are consistent with the velocity fields, with large equatorially symmetric amplitude maxima of 20–25 dbar at ±2.5° latitude, especially east of 70°E. The off-equatorial phase reversals are not particularly clear in the isotherm displacement field, although east of ~70°E there are fairly strong meridional gradients in phase at ±4°–5° latitude.

As an example to illustrate the relations among the zonal velocity, meridional velocity, and isotherm displacement fields, a snapshot of the semiannual harmonic fields in mid-January is presented (Figure 3). This snapshot shows a strong eastward flow along the equator with a maximum near 80°E (Figure 3a). In a nice illustration of continuity, to the west of that maximum meridional flow converges on the equator, feeding the eastward flow there, and to the east the meridional flow pattern diverges from the equator, taking up

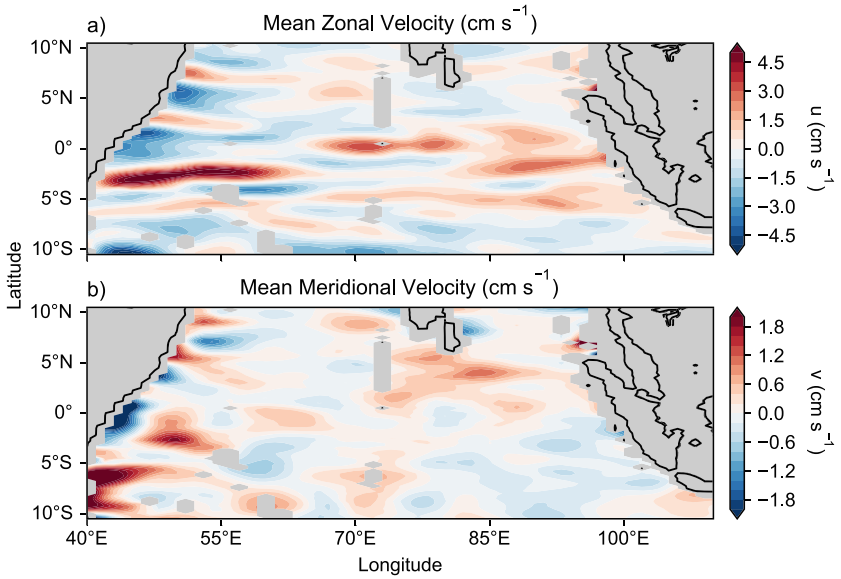

Figure 1. Equatorial Indian Ocean mean 1,000-dbar (a) zonal ($\boldsymbol{u}$) and (b) meridional ($\boldsymbol{v}$) velocity (cm·s^{-1}) from an analysis of Argo float parking depth displacements. Bathymetry shallower than 1,000 m is shaded gray.

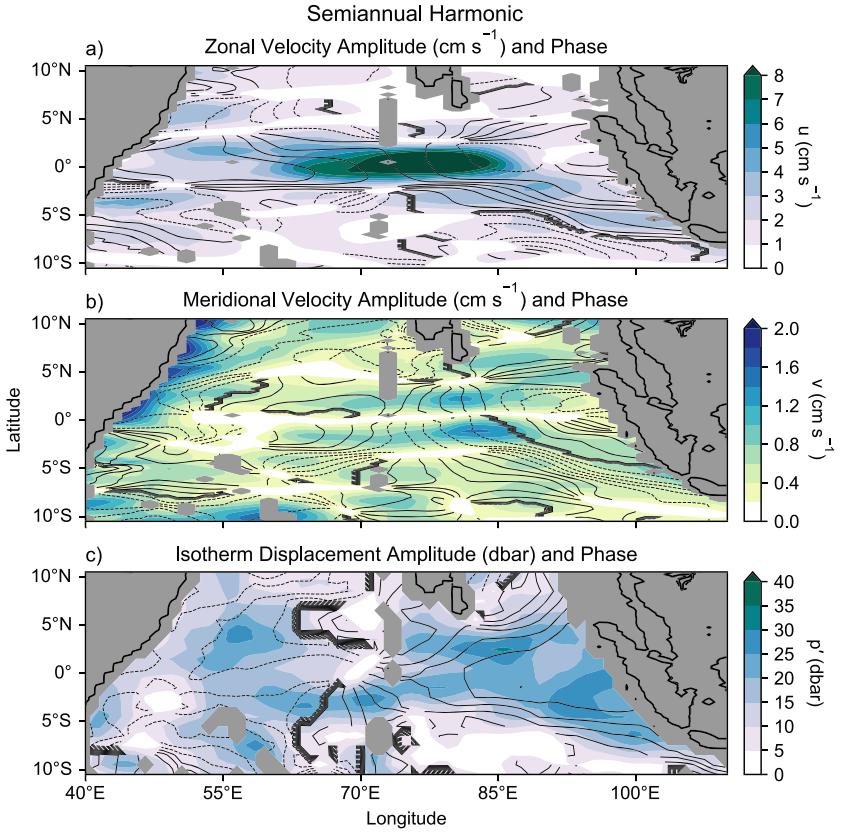

Figure 2. Semiannual harmonic amplitudes (colors) and phases (contours at 0.5-month intervals; solid, January–March and July–September; dashed, April–June and October–December for (a) zonal velocity (cm·s^{-1}), (b) meridional velocity (cm·s^{-1}), and (c) isotherm displacements (dbar). Data are mapped as in Figure 1. Phase is not shown for amplitudes less than (a) 1 cm·s^{-1}, (b) 0.2 cm·s^{-1}, and (c) 5 dbar. Bathymetry shallower than 1,000 m is shaded gray.

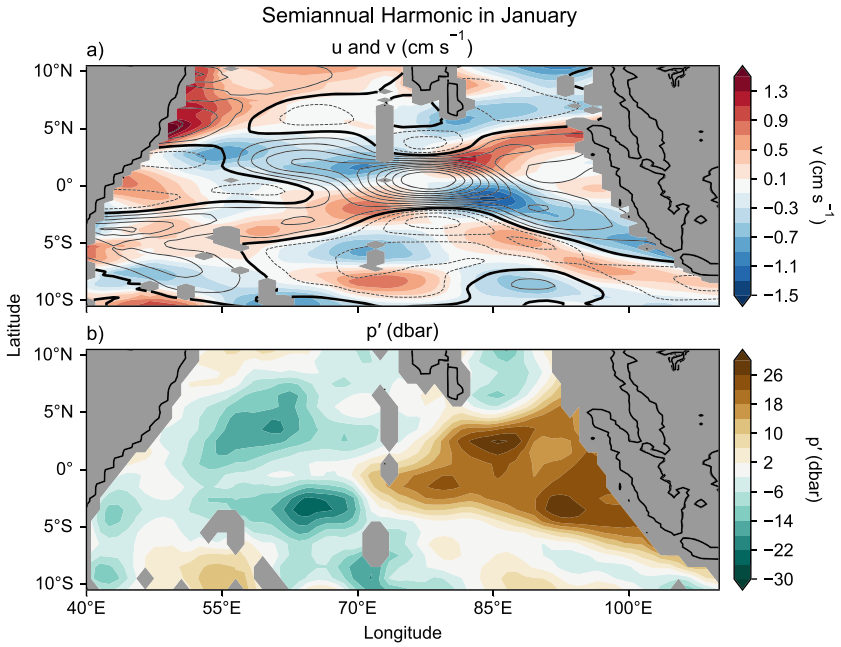

Figure 3. Mid-January snapshot of the semiannual harmonics of (a) zonal (contours; interval 1 cm·s^{-1}; thick contour, 0 cm·s^{-1}) and meridional velocity (colors; cm·s^{-1}) and (b) isotherm displacements (colors; dbar). Bathymetry shallower than 1,000 m is shaded gray.

the eastward flow. The phase reversals are also obvious in this snapshot. The presence of multiple off-equatorial phase reversals is especially clear in the meridional velocities east of 60°E (Figure 3a), where amplitudes exhibit three maxima between the equator and 10°S and up to three maxima between the equator and 10°N. However, the isotherm displacements (Figure 3b) do not exhibit multiple phase reversals that are consistent with the presence of a higher meridional mode. Instead, only one reversal at about ±4°–±5° latitude is apparent east of 85°E (Figure 3b), consistent with a first meridional mode Rossby wave. The zonal velocity structure suggests a first meridional mode Rossby wave as well, although there is some, albeit very weak, suggestion of a second phase reversal at ±5°–±6° latitude, east of 60°E (Figure 3a).

Hovmöller diagrams of the semiannual harmonic fields at 1,000 dbar are also consistent with Rossby wave physics (Figure 4). Both horizontal velocity and isotherm displacement anomalies propagate westward with time, particularly between 65°E and 90°E. West of 65°E, the westward propagation becomes unclear, aligning roughly with the beginning of the region (around 60°–65°E) in the western Indian Ocean where the spatial structure of all three fields is less coherent and amplitudes are smaller (Figure 3). The zonal phase speed of the anomalies (c_{px}), estimated from the slope of the zonal velocity anomalies in Figure 4b, is 0.56 m·s^{-1}, similar to that (c_{px} = 0.57 m·s^{-1}) found by Huang, McPhaden, et al. (2018) for their middepth zonal velocities. Calculation of the zonal wavenumber ($k = \omega/c_{px}$) yields a zonal wavelength of ~8,800 km, consistent with the larger-than-basin-scale wave suggested by the phase lines in Figure 2.

Pressure-longitude sections (Figure 5) and a time-depth Hovmöller diagram (Figure 6) of the isotherm displacement semiannual harmonics reveal the vertical structure and are broadly consistent with the presence of a vertically propagating Rossby wave. The latitudes of the sections (Figure 5; 2.5°N and 2.5°S) are chosen to be near the location of the theoretical maximum amplitudes for meridional velocity and isotherm displacements for a semiannual first meridional mode Rossby wave. Along 2.5°N (Figure 5a) and 2.5°S (Figure 5b), phase lines generally slope downward and westward from ~200 dbar at the eastern basin boundary down to 2,000 dbar between 55°E and 60°E. They largely follow the Wentzel–Kramers–Brillouin raypath of a first meridional mode Rossby wave (Figures 5a and 5b; dashed orange lines) that has been initiated via reflection at the Indian Ocean's eastern boundary (see, e.g., Figure 7 of Huang, McPhaden, et al., 2018) rather than by direct wind forcing at the surface. Phase propagation is overall upward and westward (perpendicular to the

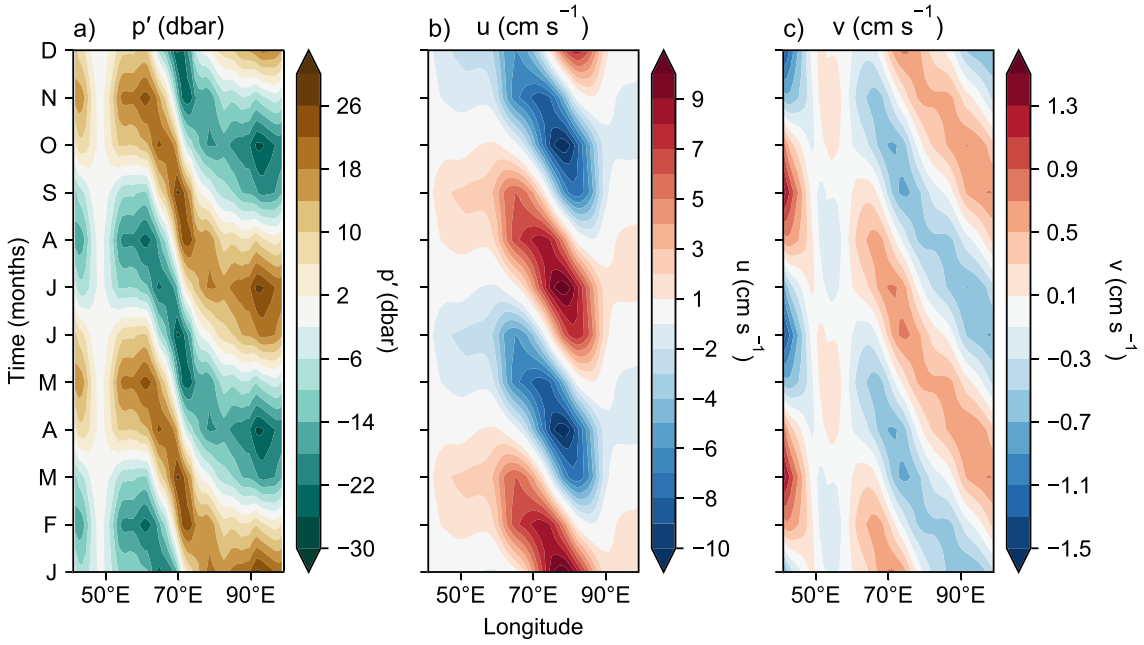

Figure 4. Hovmöller diagram of semiannual harmonics at 1,000 dbar of (a) isotherm displacements along 2.5°S (colors; dbar), (b) zonal velocity along the equator (colors; cm·s^{-1}), and (c) meridional velocity along 2.5°S (colors; cm·s^{-1}).

phase contours) as expected for a vertically propagating Rossby wave. Amplitude maxima broadly align with the downward and westward sloping phase lines, indicating the direction of energy propagation. Vertical propagation is further corroborated by the depth-time Hovmöller diagram of the isotherm displacement signals at 2.5°N, 81.5°E (Figure 6). Computation of the vertical wavenumber (m) yields a vertical wavelength estimate of ~2,700 m.

Above ~750 dbar and west of 60°E (Figure 5; orange boxes) there is another somewhat isolated amplitude maximum that appears to be separate from the signal originating in the east. In this region, the phase lines do not tilt downward as strongly especially at 2.5°S (Figure 5a), and as a result, phase propagation is oriented more strongly upward although it still maintains a westward component. Isotherm displacement pressure-latitude sections at 53.5°E, 70.5°E, and 85.5°E also suggest that the eastern and western signals are separate

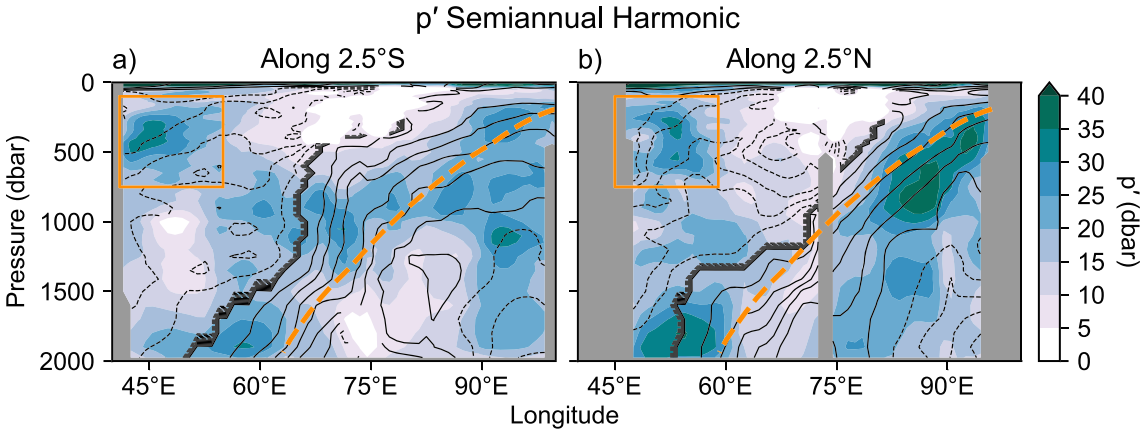

Figure 5. Isotherm displacement semiannual harmonic amplitude (colors; dbar) and phase (contours at 30° intervals) longitude-depth sections along (a) 2.5°S and (b) 2.5°N. Phase is not shown for amplitudes less than 5 dbar. Orange boxes delineate the region of the isolated amplitude maxima described in the text. Dashed orange lines indicate the WKB raypath for a first meridional mode Rossby wave computed from the mean buoyancy frequency profile in the Indian Ocean. Bathymetry is shaded gray.

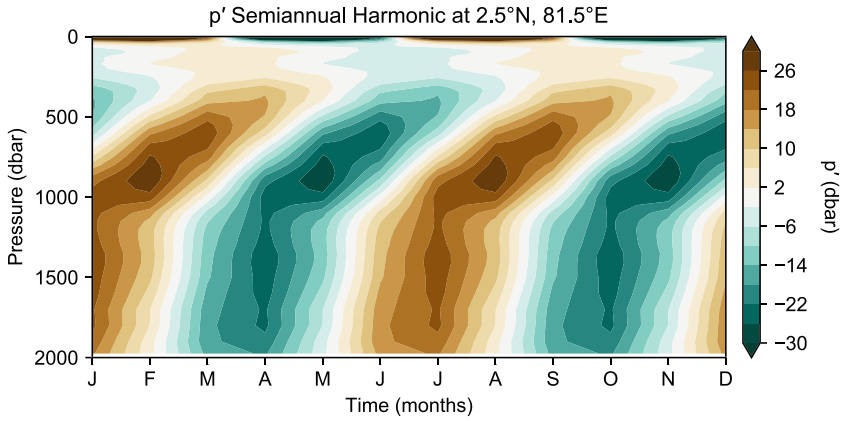

Figure 6. Time-depth Hovmöller diagram of the isotherm displacement semiannual harmonic (dbar) at 2.5°N, 81.5°E.

(Figure 7). At 85.5°E (Figure 7a) isotherm displacement amplitudes are strongest between 500 and 1,000 dbar and occur on either side of the equator at ±2.5°, with clear upward and poleward phase propagation above ~1,000 dbar. However, further west at 70.5°E (Figure 7b), these signals have largely disappeared and only a smaller amplitude maximum between 1,000 and 1,500 dbar at 2.5°S remains. Still further west at 53.5°E (Figure 7c), the isotherm displacement amplitudes and phases once again exhibit a clear meridional structure, with broad off-equatorial amplitude maxima between ~±2° and ±5° in latitude, and upward and poleward phase propagation above ~1,500 dbar. The deep amplitude maximum below this is most likely the furthest westward extent of the signal originating in the eastern basin (Figures 5 and 7a).

4. Summary and Discussion

Using horizontal velocities and isotherm displacements from Argo data, we have shown that semiannual Rossby wave signals are present in the central and eastern Indian Ocean, most clearly east of 60°–65°E. Consistent with a first meridional mode Rossby wave, 1,000-dbar zonal velocities are maximal on the equator with off-equatorial phase reversals (at ±2.5° in latitude) that are colocated with meridional velocity and isotherm displacement amplitude extrema (Figures 2 and 3) at the same depth. All three fields exhibit westward propagation between ~65°E and 90°E (Figure 4).

Pressure-longitude and pressure-latitude isotherm displacement sections down to 2,000 dbar suggest that the signals at 1,000-dbar are the result of a vertically propagating Rossby wave. Phase lines are oriented downward and westward across the basin, indicating upward and westward propagation of phase (Figure 5) that is confirmed by a time-depth Hovmöller diagram of the isotherm displacements at 2.5°N, 81.5°E (Figure 6). Amplitude maxima generally follow lines of constant phase, indicating downward and westward energy propagation (Figure 5). There is some indication of a separate area of large amplitude in the far western Indian Ocean above 750 dbar (Figure 5; orange boxes) that is corroborated by the signals at 53.5°E (Figure 7c). There the amplitudes are equatorially symmetric and show upward phase propagation especially above 750 dbar. This potentially distinct amplitude beam could be the result of a vertically propagating, semiannual Rossby wave that is forced by variations in the winds off of Somalia. Similar to those in the east-central equatorial Indian Ocean, the winds off of Somalia reverse twice a year in accordance with the southwest and northeast monsoons (Schott et al., 2009), resulting in the propagation of planetary waves that have been linked to the reversal of the Somali Current (e.g., Lighthill, 1969). Short waves—resulting from incident long-wave reflection at the Indian Ocean's western boundary—are dynamically important in this region (e.g., Visbeck & Schott, 1992) as well and may also contribute to the large amplitudes we find there.

Our results are consistent with previous studies (e.g., Luyten & Roemmich, 1982; Huang, Han, et al., 2018; Huang, McPhaden, et al., 2018) that have demonstrated that strong semiannual variations in deep zonal velocities are in part the result of a vertically propagating, first meridional mode Rossby wave. The zonal velocity semiannual signals presented here have been described previously using Argo data (Davis, 2005)

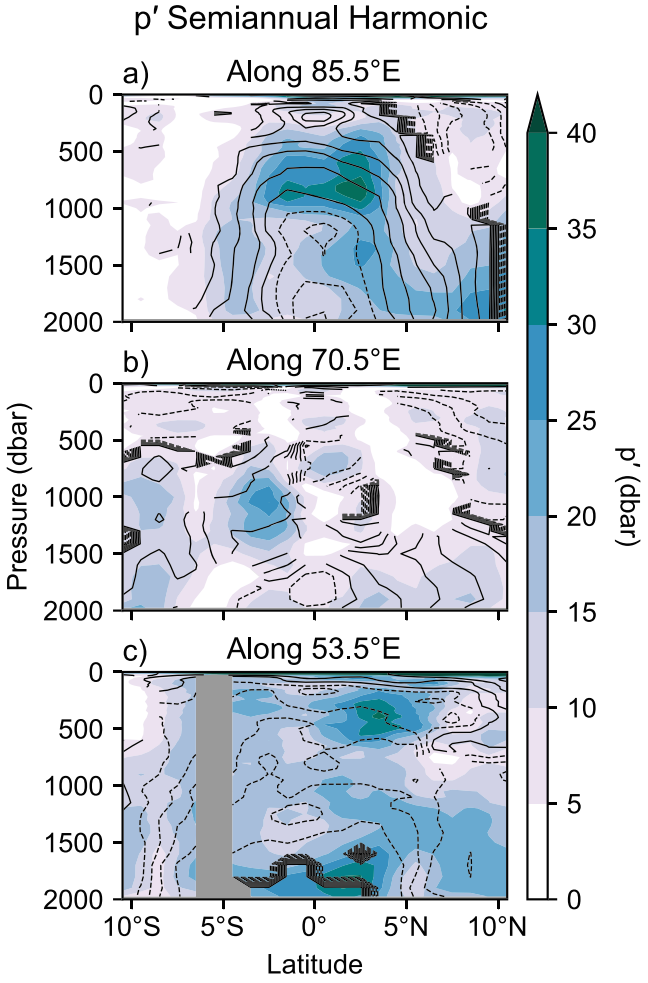

Figure 7. Isotherm displacement semiannual harmonic amplitude (colors; dbar) and phase (contours at 30° intervals) latitude-depth sections along (a) 85.5°E, (b) 70.5°E, and (c) 53.5°E. Phase is not shown for amplitudes less than 5 dbar. Bathymetry is shaded gray.

and have been revisited more recently with a focus on the middepth (500–1,500 m) equatorial Indian Ocean (Huang, Han, et al., 2018; Huang, McPhaden, et al., 2018). However, we provide a more complete picture of the semiannual variations by including analyses of the meridional velocity (which are novel to the best of our knowledge) and isotherm displacements, both of which indicate the presence of a vertically propagating Rossby wave (Figures 2–7) as well. Using mooring data in the western Indian Ocean, Luyten and Roemmich (1982) did not find evidence of semiannual variations in the meridional velocity, but this is likely because the moorings were within 1° of the equator, where Rossby wave-driven meridional velocity anomalies should be and are (Figures 2b and 3b) small. The eastward extent of the moorings was also 62°E, which coincides with the furthest westward extent of the largest and clearest meridional velocity semiannual variations shown here.

Although vertical propagation is clear in our results, it is also likely that basin resonance modulates the observed semiannual signals. Like Rossby waves, the semiannual basin resonance in the Indian Ocean also propagates westward (e.g., Han et al., 2011), although it is faster than pure Rossby waves because it is a combination of Rossby and Kelvin waves. The resulting Kelvin wave phase speed ($c = N/m$) computed from depth-averaged N ($0.0039\ s^{-1}$) and our estimate of m ($2\pi/2{,}700\ m^{-1}$) is $1.68\ m{\cdot}s^{-1}$, which is very close to that of a second baroclinic mode Kelvin wave ($1.67\ m{\cdot}s^{-1}$; Han et al., 2011; Huang, Han, et al., 2018). It is these second baroclinic mode waves that contribute most strongly to Indian Ocean basin resonance at semiannual period (e.g., Jensen, 1993; Huang, Han, et al., 2018). Our 1,000-dbar zonal velocity anomaly magnitudes also compare somewhat more favorably to those resulting from basin resonance in Huang, Han, et al. (2018) rather than those resulting from vertically propagating waves in Huang, McPhaden, et al. (2018).

The 1,000-dbar meridional velocity semiannual harmonic also suggests the presence of higher-than-first meridional mode Rossby wave energy (Figures 2b and 3a), with three distinct amplitude maxima between the equator and 10°N and three more distinct amplitude maxima between the equator and 10°S (Figure 3a). The latitudes of the meridional velocity phase reversals (amplitude zero crossings) align well with those theoretically predicted for a fifth meridional mode Rossby wave (not shown). However, a fifth-mode structure is not found in either the isotherm displacement or the 1,000-dbar zonal velocity semiannual harmonic fields, both of which suggest a first meridional mode Rossby wave in agreement with Luyten and Roemmich (1982) and Huang, McPhaden, et al. (2018). It is thus unclear what leads to this particular latitudinal structure in the meridional velocities (Figure 3a). Further investigation, perhaps with an idealized model, seems necessary in order to understand the mechanisms underlying the meridional velocity spatial patterns.

Acknowledgments
The YoMaHa'07 data set (Lebedev et al., 2007) is available at http://apdrc.soest.hawaii.edu/projects/yomaha/. The Roemmich and Gilson (2009) Argo Climatology is available at http://sio-argo.ucsd.edu/RG_Climatology.html. H. Z. was funded by the Joint Institute for the Study of the Atmosphere and Ocean (JISAO) under NOAA Cooperative Agreement NA15OAR4320063. G. C. J. was funded by the Climate Observation Division, Climate Program Office, National Oceanic and Atmospheric Administration (NOAA), the U.S. Department of Commerce, and NOAA Research. All figures were created using Python's matplotlib plotting package. PMEL contribution number 4980.

References

Cane, M. A., & Moore, D. W. (1981). A note on low-frequency equatorial basin modes. *Journal of Physical Oceanography*, *11*, 1578–1584. https://doi.org/10.1175/15200485(1981)011<1578:ANOLFE>2.0.CO;2

Chen, G., Han, W., Li, Y., Wang, D., & McPhaden, M. J. (2015). Seasonal-to-interannual time-scale dynamics of the equatorial undercurrent in the Indian Ocean. *Journal of Physical Oceanography*, *45*, 1532–1553. https://doi.org/10.1175/JPO-D-14-0225.1

Chen, G., Han, W., Li, Y., Yao, J., & Wang, D. (2019). Intraseasonal variability of the Equatorial Undercurrent in the Indian Ocean. *Journal of Physical Oceanography*, *49*, 85–101. https://doi.org/10.1175/JPO-D-18-0151.1

Cravatte, S., Kessler, W. S., & Marin, F. (2012). Intermediate zonal jets in the tropical Pacific Ocean observed by Argo floats. *Journal of Physical Oceanography*, *42*, 1475–1485. https://doi.org/10.1175/JPO-D-11-0206.1

Davis, R. E. (2005). Intermediate-depth circulation of the Indian and South Pacific Oceans measured by autonomous floats. *Journal of Physical Oceanography*, *35*, 683–707. https://doi.org/10.1175/JPO2702.1

Dengler, M., & Quadfasel, D. (2002). Equatorial deep jets and abyssal mixing in the Indian Ocean. *Journal of Physical Oceanography*, *32*, 1165–1180. https://doi.org/10.1175/1520-0485(2002)032<1165:EDJAAM>2.0.CO;2
Gent, P. R., O'Neill, K., & Cane, M. A. (1983). A model of the semiannual oscillation in the equatorial Indian Ocean. *Journal of Physical Oceanography*, *13*, 2148–2160. https://doi.org/10.1175/1520-0485(1983)013<2148:AMOTSO>2.0.CO;2
Han, W., McCreary, J. P., Anderson, D. L., & Mariano, A. J. (1999). Dynamics of the eastern surface jets in the equatorial Indian Ocean. *Journal of Physical Oceanography*, *29*, 2191–2209. https://doi.org/10.1175/1520-0485(1999)029<2191:DOTESJ>2.0.CO;2
Han, W., McCreary, J. P., Masumoto, Y., Vialard, J., & Duncan, B. (2011). Basin resonances in the equatorial Indian Ocean. *Journal of Physical Oceanography*, *41*, 1252–1270. https://doi.org/10.1175/2011JPO4591.1
Huang, K., Han, W., Wang, D., Wang, W., Xie, Q., Chen, J., & Chen, G. (2018). Features of the equatorial intermediate current associated with basin resonance in the Indian Ocean. *Journal of Physical Oceanography*, *48*, 1333–1347. https://doi.org/10.1175/JPO-D-17-0238.1
Huang, K., McPhaden, M. J., Wang, D., Wang, W., Xie, Q., Chen, J., et al. (2018). Vertical propagation of middepth zonal currents associated with surface wind forcing in the equatorial Indian Ocean. *Journal of Geophysical Research: Oceans*, *123*, 7290–7307. https://doi.org/10.1029/2018JC013977
Iskandar, I., Masumoto, Y., & Mizuno, K. (2009). Subsurface equatorial zonal current in the eastern Indian Ocean. *Journal of Geophysical Research*, *114*, C06005. https://doi.org/10.1029/2008JC005188
Jensen, T. G. (1993). Equatorial variability and resonance in a wind-driven Indian Ocean model. *Journal of Geophysical Research*, *98*(C12), 22,533–22,552. https://doi.org/10.1029/93JC02565
Kessler, W. S., & McCreary, J. P. (1993). The annual wind-driven Rossby wave in the subthermocline equatorial Pacific. *Journal of Physical Oceanography*, *23*(6), 1192–1207. https://doi.org/10.1175/1520-0485(1993)023¡1192:TAWDRW¿2.0.CO;2
Knox, R. A. (1974). Reconnaissance of the Indian Ocean equatorial undercurrent near Addu Atoll. *Deep Sea Research and Oceanographic Abstracts*, *21*(2), 123–129. https://doi.org/10.1016/0011-7471(74)90069-2
Knox, R. A. (1976). On a long series of measurements of Indian Ocean equatorial currents near Addu Atoll. *Deep Sea Research and Oceanographic Abstracts*, *23*(3), 211–221. https://doi.org/10.1016/0011-7471(76)91325-5
Knox, R. A., & Anderson, D. L. T. (1985). Recent advances in the study of the low-latitude ocean circulation. *Progress in Oceanography*, *14*, 259–317. https://doi.org/10.1016/0079-6611(85)90014-X
Lebedev, K. V., Yoshinari, H., Maximenko, N. A., & Hacker, P. W. (2007). YoMaHa'07: Velocity data assessed from trajectories of Argo floats at parking level and at the sea surface, IPRC Tech. Rep. 4(2)
Lighthill, M. J. (1969). Dynamic response of the Indian Ocean to onset of the Southwest Monsoon. *Philosophical Transactions of the Royal Society A*, *265*(1159), 45–92. https://doi.org/0.1098/rsta.1969.0040
Luyten, J. R., & Roemmich, D. H. (1982). Equatorial currents at semi-annual period in the Indian Ocean. *Journal of Physical Oceanography*, *12*, 406–413. https://doi.org/10.1175/1520-0485(1982)012<0406:ECASAP>2.0.CO;2
Luyten, J. R., & Swallow, J. C. (1976). Equatorial undercurrents. *Deep Sea Research and Oceanographic Abstracts*, *23*(10), 999–1001. https://doi.org/10.1016/0011-7471(76)90830-5
McPhaden, M. (1982). Variability in the central equatorial Indian Ocean. I: Ocean dynamics. *Journal of Marine Research*, *40*, 157–176.
McPhaden, M. J., Wang, Y., & Ravichandran, M. (2015). Volume transports of the Wyrtki jets and their relationship to the Indian Ocean Dipole. *Journal of Geophysical Research: Oceans*, *120*, 5302–5317. https://doi.org/10.1002/2015JC010901
Moore, D. W., & McCreary, J. P. (1990). Excitation of intermediate-frequency equatorial waves at a western ocean boundary: With application to observations from the Indian Ocean. *Journal of Geophysical Research*, *95*(C4), 5219–5231. https://doi.org/10.1029/JC095iC04p05219
Nagura, M., & McPhaden, M. J. (2008). The dynamics of zonal current variations in the central equatorial Indian Ocean. *Geophysical Research Letters*, *35*, L23603. https://doi.org/10.1029/2008GL035961
Nagura, M., & McPhaden, M. J. (2010a). Wyrtki jet dynamics: Seasonal variability. *Journal of Geophysical Research*, *115*, C07009. https://doi.org/10.1029/2009JC005922
Nagura, M., & McPhaden, M. J. (2010b). Dynamics of zonal current variations associated with the Indian Ocean dipole. *Journal of Geophysical Research*, *115*, C11026. https://doi.org/10.1029/2010JC006423
Nagura, M., & McPhaden, M. J. (2016). Zonal propagation of near-surface zonal currents in relation to surface wind forcing in the equatorial Indian Ocean. *Journal of Physical Oceanography*, *46*, 3623–3638. https://doi.org/10.1175/JPO-D-16-0157.1
Nyadjro, E. S., & McPhaden, M. J. (2014). Variability of zonal currents in the eastern equatorial Indian Ocean on seasonal to interannual time scales. *Journal of Geophysical Research: Oceans*, *119*, 7969–7986. https://doi.org/10.1002/2014JC010380
Ponte, R. M., & Luyten, J. (1990). Deep velocity measurements in the western equatorial Indian Ocean. *Journal of Physical Oceanography*, *20*, 44–52. https://doi.org/10.1175/1520-0485(1990)020<0044:DVMITW>2.0.CO;2
Reppin, J., Schott, F. A., Fischer, J., & Quadfasel, D. (1999). Equatorial currents and transports in the upper central Indian Ocean: Annual cycle and interannual variability. *Journal of Geophysical Research*, *104*(C7), 15,495–15,514. https://doi.org/10.1029/1999JC900093
Reverdin, G. (1987). The upper equatorial Indian Ocean. The climatological seasonal cycle. *Journal of Physical Oceanography*, *17*, 903–927. https://doi.org/10.1175/1520-0485(1987)017<0903:TUEIOT>2.0.CO;2
Ridgway, K. R., Dunn, J. R., & Wilkin, J. L. (2002). Ocean interpolation by four-dimensional weighted least squares—Application to the waters around Australasia. *Journal of Atmospheric and Oceanic Technology*, *19*, 1357–1375. https://doi.org/10.1175/1520-0426(2002)019<1357:OIBFDW>2.0.CO;2
Roemmich, D., & Gilson, J. (2009). The 2004–2008 mean and annual cycle of temperature, salinity, and steric height in the global ocean from the Argo program. *Progress in Oceanography*, *82*(2), 81–100. https://doi.org/10.1016/j.pocean.2009.03.004
Schott, F. A., & McCreary, J. P. (2001). The monsoon circulation of the Indian Ocean. *Progress in Oceanography*, *51*(1), 1–123. https://doi.org/10.1016/S0079-6611(01)00083-0
Schott, F. A., Xie, S.-P., & McCreary, J. P. (2009). Indian Ocean circulation and climate variability. *Reviews of Geophysics*, *47*, RG1002. https://doi.org/10.1029/2007RG000245
Sengupta, D., Senan, R., Goswami, B. N., & Vialard, J. (2007). Intraseasonal variability of equatorial Indian Ocean zonal currents. *Journal of Climate*, *20*, 3036–3055. https://doi.org/10.1175/JCLI4166.1
Visbeck, M., & Schott, F. (1992). Analysis of seasonal current variations in the western equatorial Indian Ocean: Direct measurements and GFDL model comparison. *Journal of Physical Oceanography*, *22*, 1112–1128. https://doi.org/10.1175/15200485(1992)022<1112:AOSCVI>2.0.CO;2
Wyrtki, K. (1973). An equatorial jet in the Indian Ocean. *Science*, *181*(4096), 262–264. https://doi.org/10.1126/science.181.4096.262
Youngs, M. K., & Johnson, G. C. (2015). Basin-wavelength equatorial deep jet signals across three oceans. *Journal of Physical Oceanography*, *45*, 2134–2148. https://doi.org/10.1175/JPO-D-14-0181.1

Yuan, D., & Han, W. (2006). Roles of equatorial waves and western boundary reflection in the seasonal circulation of the equatorial Indian Ocean. *Journal of Physical Oceanography*, *36*, 930–944. https://doi.org/10.1175/JPO2905.1

Zhang, D., McPhaden, M. J., & Lee, T. (2014). Observed interannual variability of zonal currents in the equatorial Indian Ocean thermocline and their relation to Indian Ocean Dipole. *Geophysical Research Letters*, *41*, 7933–7941. https://doi.org/10.1002/2014GL061449